International Journal of Fatigue 95 (2017) 236–242

Contents lists available at ScienceDirect

International Journal of Fatigue

journal homepage: www.elsevier.com/locate/ijfatigue

Short-beam shear fatigue behavior of fiber metal laminate (Glare)

Héctor G. Kotik [a,b,*], Juan E. Perez Ipiña [a]

[a] Grupo Mecánica de Fractura, Universidad Nacional del Comahue/CONICET, Buenos Aires 1400, Neuquén CP 8300, Argentina
[b] Universidad Nacional del Sur, Departamento de ingeniería, Avenida Alem 1253, Bahía Blanca B8000CPB, Argentina

ARTICLE INFO

Article history:
Received 26 August 2016
Received in revised form 28 October 2016
Accepted 2 November 2016
Available online 2 November 2016

Keywords:
Short-beam shear fatigue
Glare
Fiber metal laminate
Interlaminar shear

ABSTRACT

Interlaminar shear stresses have an important role in behavior of fiber metal laminates (FMLs). Low interlaminar shear strength in the crack bridging mechanism of these materials is considered beneficial because produces delamination and this prevents fiber failure; although when this strength is too low excessive delamination can occur, leading to a less efficient mechanism. This strength also has important roles in fatigue crack nucleation of internal laminae and in cases where the material is subject to shear stresses. This paper studied quasi-static and fatigue ($R = 0.1$; 5 Hz) interlaminar shear behavior of a commercial FML (Glare 1 3/2) employing the short-beam shear (SBS) test in longitudinal and transversal orientations. Failure modes and the limitations of the SBS test to characterize the interlaminar shear fatigue behavior are described and discussed.

1. Introduction

Glare® laminates are part of the fiber metal laminates (FMLs) family of structural composite materials. They were created and developed mainly for aeronautical applications at the Technical University of Delft, Netherlands [1,2]. These orthotropic materials were designed aiming to produce damage-tolerant thin sheets with high specific strength. FML materials have shown very good properties and characteristics for different requests [3]. The main characteristic of Glare laminates, as well as the whole FML family, is their very low fatigue crack propagation rate if compared to traditional aeronautical Al alloys [2].

Shear stresses and the shear strength both inter and intralaminar have an important role in the fatigue [4] and fracture [5] behavior of FML. *E.g.*, the high resistance to fatigue crack growth in FMLs is largely due to the crack bridging mechanism where a part of the fatigue loads are transferred over the cracks in the aluminum layers by the unbroken fiber layers, as Alderliesten [2] explains. Cyclic shear stresses in the interface metal-fiber/matrix transfer these loads and they cause delamination at the interface that reduces the fiber bridging stress and it prevents fiber failure [6]. However, when delamination is too large, the bridging stress in the fibers decreases and the bridging mechanism is less efficient. From the point of view of the crack nucleation stage, this delamination delays the crack initiation in the interior metal layers. Auffret and Gennai [2] commented that this delamination occurs more frequently by factors among which is a low shear strength of the adhesive layer (interface).

On the other hand, delamination can be harmful for other characteristics and properties of the material. When the composite is subject to interlaminar shear stresses (*e.g.* bending moments), this relatively low shear strength can contribute to interlaminar failure both by quasi-static or fatigue loads.

This paper gives information about quasi-static and fatigue interlaminar shear responses of a commercial FML (Glare 1 3/2) employing the SBS test. Moreover, it discusses the failure mode of the specimens and the limitations of the SBS test to characterize the interlaminar shear fatigue behavior.

2. Material and methods

The material used in this research was Glare 1 3/2. It consists in three 7475-T76 alloy layers and two S-glass reinforced epoxy prepreg layers. The glass-fiber direction is oriented along the rolling direction of the metal alloy layers as it is shown in Fig. 1.

Some characteristics and mechanical properties of the material are presented in Table 1.

Material was cut in longitudinal and transversal direction with a circular blade saw of 50 mm diameter and 0.2 mm thickness, table feed 30 mm/min and no cooling. Specimen dimensions maintained the geometric ratio proposed in ASTM D2344-13 [8]: specimen length-to-thickness ratio $l/t = 6$, while the width-to-thickness ratio $b/t = 2.0$. The specimen surfaces in the planes 1–3 and 2–3

* Corresponding author at: Grupo Mecánica de Fractura, Universidad Nacional del Comahue/CONICET, Buenos Aires 1400, Neuquén CP 8300, Argentina.
E-mail address: hector.kotik@fain.uncoma.edu.ar (H.G. Kotik).

http://dx.doi.org/10.1016/j.ijfatigue.2016.11.001
0142-1123/

Nomenclature

b	specimen width	S	standard deviation
E	tensile modulus of elasticity	SBS	short-beam shear
FML	fiber metal laminate	α	significance level
F^{sbs}	quasi-static short-beam strength	δ	displacement of the loading nose
t	specimen thickness	δmax	maximum displacement of the loading nose in one cycle
l	specimen length	F^{uts}	ultimate tensile strength
N	number of cycles	F^{ys}	tensile yield stress
N_f	number of cycles at failure or SBS fatigue life of a specimen	τ_a	shear stress amplitude
P	force	$\tau^{sbs}_{(i)}$	SBS stress value observed at ith data point in one cycle
$P_{(i)}$	force at ith data point observed during the fatigue test	τ^{sbs}_{max}	maximum SBS stress value observed in one cycle
R	shear stress-ratio	τ^{sbs}_{min}	minimum SBS stress value observed in one cycle
R^2	coefficient of determination		

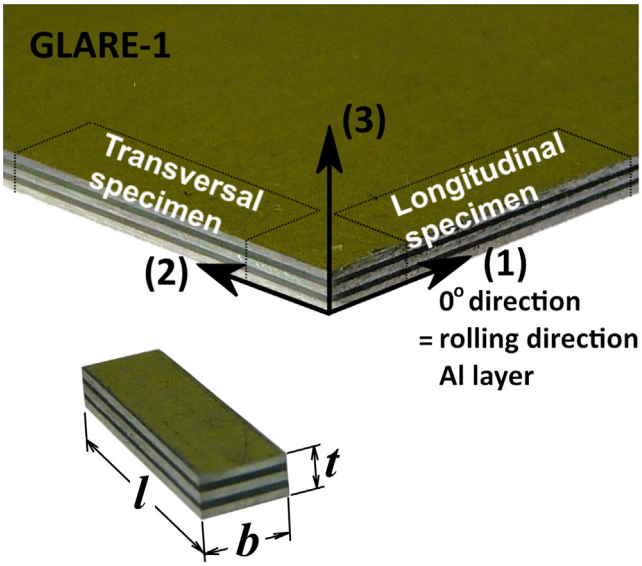

Fig. 1. Material, cutting direction and nomenclature of the specimens.

Table 1
Characteristics and mechanical properties of Glare 1 [7].

Material	Glare 1		
Lay-up	3/2	F_1^{uts} (MPa)	1282
Fibers	S-glass	F_2^{uts} (MPa)	352
Al alloy	7475-T76	E_1 (GPa)	64
Post-stretch (%)	0.4	E_2 (GPa)	49
F_1^{ys} (MPa)	545	ρ (kg/m^3)	2520
F_2^{ys} (MPa)	338	t (mm)	1.42
Metallic percentage (Vol)	67.9		

(Fig. 1) were sanded with 240, 500 and 1200 grid size sandpapers to remove cutting marks.

The force was measured with a 1.3 kN capacity load cell and the loading nose displacement was measured with a LVDT Omega 500 (2.5 mm stroke). The tests were monitored with a USB digital microscope of 2.0 Mpx and 50× magnification. Tests were conducted at a standard laboratory atmosphere (23 °C, 50% RH).

The SBS stress at ith data point corresponding to the neutral axis of the beam was calculated using Eq. (1).

$$\tau^{sbs}_{(i)} = \frac{3}{4}\frac{P_{(i)}}{bt} \tag{1}$$

In quasi-static tests, the load was applied monotonically and the $P_{(i)}$ value corresponds to the maximum load measured during the test. These results of quasi-static test were indicated as F^{sbs} [8]. The shear stress-ratio (R) was estimated according to Eq. (2) and shear stress amplitude (τ_a) with Eq. (3).

$$R = \frac{\tau^{sbs}_{min}}{\tau^{sbs}_{max}} \tag{2}$$

$$\tau_a = \frac{\tau^{sbs}_{max} - \tau^{sbs}_{min}}{2} \tag{3}$$

Quasi-static tests were performed with a universal testing machine EMIC DL 2000 and the crosshead speed was 0.5 mm/min.

A special purpose fatigue machine that produces constant amplitude load cycles was used in the fatigue tests [9]. This test machine and the test device are shown in Fig. 2. All tests were performed at a loading frequency of 5 Hz, sinusoidal waveform and $R = 0.1$. Six τ_a levels were selected for both longitudinal and transversal specimens.

The test device consists in a three-point bending rig. The used diameters of support rollers and the loading nose were 1 and 2 mm respectively. A span-to-thickness ratio of 4.0 was employed in 18 quasi-static and 58 fatigue tests. A span-to-thickness ratio of 0.7 was used in 5 fatigue tests to evaluate the indentation effect in the fatigue life.

The specimen loss of stiffness was used as indicator of damage and the specimen collapse was used as failure condition. The maximum displacement of the loading nose in one cycle (δmax) was associated to the stiffness loss of the specimen [10]. The fatigue tests were conducted up to the specimen failure or stopped beyond 10^6 cycles.

Fitted curves were plotted together to the fatigue data. They have the form

$$\tau_a = \tau_0 N^{-1/k} \tag{4}$$

where τ_0 and k are fitting coefficients [11,12].

3. Results

The F^{sbs} results of the longitudinal specimens were: media 81.6 MPa, *SD* 3.0 MPa and *CV* 3.68%. The values corresponding to transversal specimens were: media 72.5 MPa, *SD* 3.2 MPa and *CV* 4.41%.

Results of all SBS fatigue tests are presented in Table 2 and are shown in a τ_a-log N_f graph in Fig. 3a. The circles correspond to longitudinal specimens while squares correspond to transversal specimens. The failure mode of each specimen is indicated with different marks in the circle or the square. Photographs of an untested specimen and specimens after testing are shown from

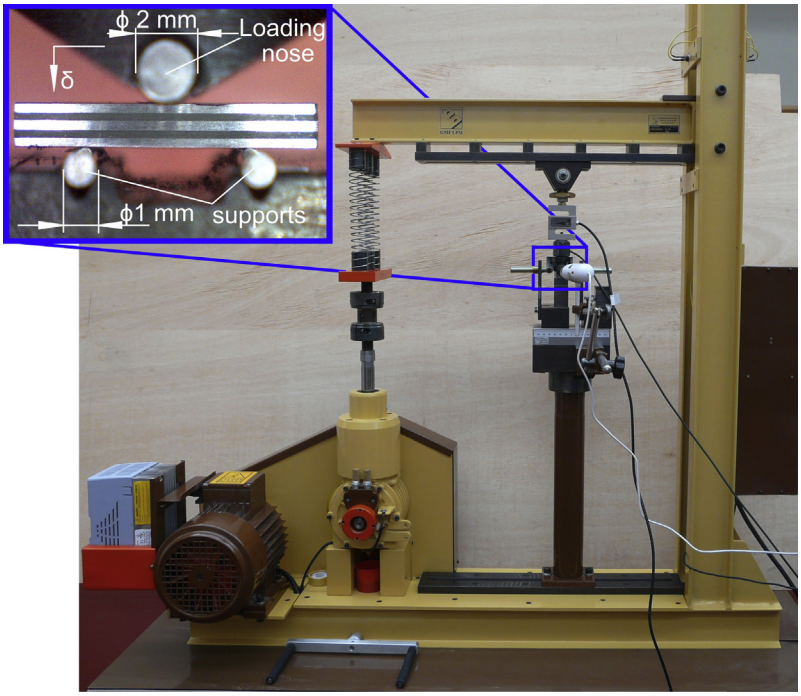

Fig. 2. Test machine and test device.

Table 2
Fatigue life and type of failure of the specimens.

Longitudinal specimens			Transversal specimens		
τ_a (MPa)	N_f (cycles)	Failure type	τ_a (MPa)	N_f (cycles)	Failure type
27.1	2350	*e*	24.1	5510	*h*
27.1	2860	*e*	24.1	3150	*f*
27.1	2360	*e*	24.1	3500	*f*
27.1	2330	*e*	24.1	2180	*f*
25.2	10,050	*e*	24.1	2190	*f*
25.2	10,160	*e*	22.5	6660	*h*
25.2	5010	*e*	22.5	8110	*g*
25.2	5190	*e*	22.3	19,150	*h*
25.2	5300	*e*	22.5	9940	*f*
23.4	21,420	*e*	22.5	4370	*f*
23.4	23,270	*e*	20.9	49,880	*g*
23.4	27,680	*e*	20.9	35,240	*g*
23.4	23,690	*e*	20.9	35,320	*h*
23.4	15,770	*e*	20.9	18,110	*g*
21.6	67,900	*e*	20.9	42,670	*g*
21.6	35,500	*e*	20.6	35,570	*i*
21.6	67,260	*h*	19.2	35,090	*h*
21.6	57,660	*e*	19.2	375,750	*g*
21.6	68,030	*e*	19.1	34,130	*g*
20.2	135,170	*e*	19.1	169,140	*h*
20.2	134,240	*e*	19.1	84,760	*h*
20.2	194,300	*e*	19.0	51,015	*g*
20.2	186,850	*e*	18.6	246,930	*g*
20.2	120,880	*e*	17.9	52,430	*i*
18.8	2,681,190	*e*	17.9	1,196,900	*i*
18.8	1,084,960	*e*	17.9	388,450	*i*
18.8	4,109,660	*e*	17.9	726,100	*g*
18.8	3,008,710	Run-out	17.9	773,060	*i*
18.8	2,429,290	Run-out	17.9	257,090	*i*

f Interlaminar shear damage.
e, *g* Interlaminar shear and subsequent crack in the middle span of the tension face.
h Interlaminar shear and subsequent crack in the middle span of the tension face. When the beam collapse, a cracks next the supports were observed.
i Crack initiated in a support and subsequent collapse of the beam with interlaminar damage.

Fig. 3b to i. Fig. 3b shows a transversal SBS specimen before testing. Failure mode of quasi-static tests for a longitudinal and a transversal specimen are shown in Fig. 3c and d respectively. All quasi-static specimens presented interlaminar shear failure mode. Fatigue specimens presented four different types of failure during the tests which were denominated as type *e*, *f*, *g*, *h* and *i*, in accordance with the photograph of Fig. 3. The damage processes observed are described as follows.

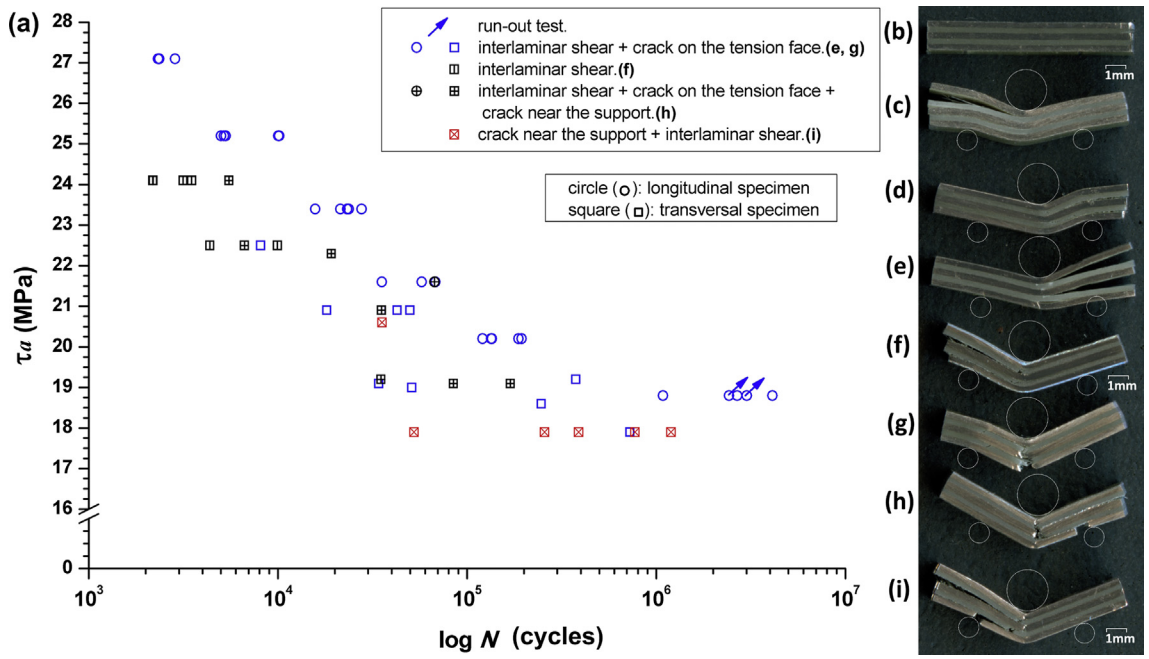

Fig. 3. (a) Graph τ_a–log N with all results of SBS fatigue tests. Photographs of (b) a specimen before testing, (c and d) failure modes of quasi-static tests, (e–i) failure modes of fatigue tests.

In type *f*, an interlaminar crack grew along the specimen and it produced the collapse of the beam. These specimens presented only interlaminar shear damage as can be seen in Fig. 3f.

In the types *e* and *g* interlaminar damage in the glass-epoxy layer was observed in first place. However, a crack nucleated in middle span at the tension face grew through the aluminum layer up to produce the collapse of the beam. A broken longitudinal specimen with this failure can be observed in Fig. 3e and for a transversal specimen in Fig. 3g.

The type *h* presented firstly interlaminar shear damage. While the interlaminar damage was increasing, two cracks were nucleated: a crack in the middle span and another in the glass/epoxy-aluminum interface next to a support. This last crack grew through the aluminum layer toward the support. When the crack in the middle span reached the glass/epoxy layer, the specimen collapsed and the other crack grew toward the support. Therefore, the failed specimen presented interlaminar shear damage and two cracks, one in the middle span and the other next to a support as can be seen in Fig. 3h.

In the type *i*, a crack was nucleated in the indentation of a support and it grew through the aluminum layer until to reach the glass-epoxy layer. The crack produced interlaminar damage and the collapse of the beam as can be seen in Fig. 3i.

The run-out specimens showed the typical indentation marks of all SBS fatigue specimens. Interlaminar damage or other damage mechanisms were not observed when the tests were stopped.

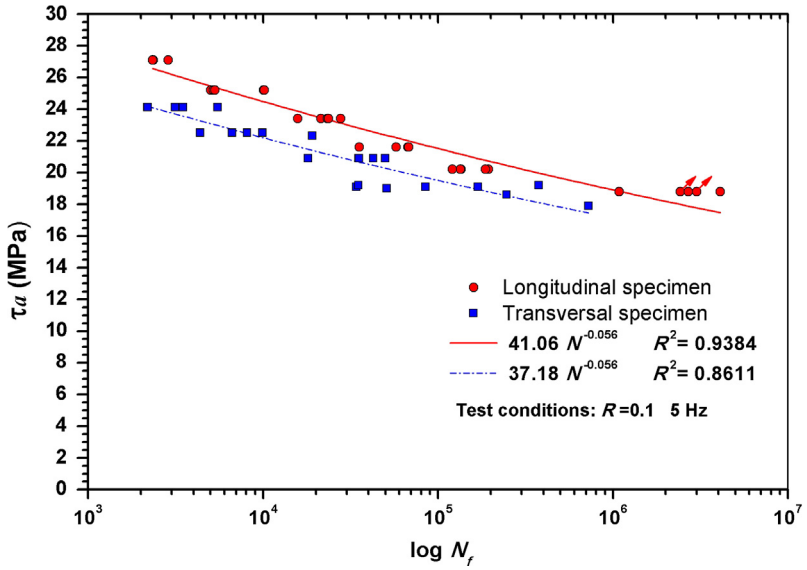

Fig. 4. Graph τ_a–log N_f of specimens with failure type *e*, *f*, *g* and *h*.

The failures type *e*, *f*, *g* and *h* are plotted in a τ_a-log N_f graph in Fig. 4. Also, the fitted curves and R^2 for both SBS fatigue specimens are shown.

The δmax-N/N_f curves of longitudinal and transversal specimens are presented in Fig. 5. These curves correspond to one specimen by stress level. Two graphs δmax *vs. N* of longitudinal specimens for two span-to-thickness values are shown in Fig. 6. The first one shows the results of two specimens at τ_a = 25.2 MPa, while the second one shows the results for τ_a = 20.2 MPa.

4. Discussion

The material thickness (1.4 mm) is smaller than the values commonly used in both SBS quasi-static and SBS fatigue tests [8,13–16,10]. The diameters of the rollers (supports and loading nose) are smaller than those used in standardized quasi-static tests [8,17]. This change allows to use a span-to-thickness ratio of 4.0 and this prevents compression jamming when the specimens suffers stiffness loss.

The F^{sbs} values for both longitudinal (81.6 MPa) and transversal (72.5 MPa) specimens are similar to values of carbon fiber reinforced epoxy composites [18]. The authors of the present study did not find values of F^{sbs} for Glare 1. Park et al. [19] reported F^{sbs} results of Glare 2 5/4–0.4 that are approximately 25% lower than the longitudinal results in this study. This comparison is limited to a test device with different roller diameters [20], speed of testing and Glare type. However, Glare 2 has the same fiber orientation and fiber/epoxy composite. Botelho et al. [18] report values of F^{sbs} = 40 MPa without specifying the Glare type and orientation.

Comparing results between the two orientations, the longitudinal F^{sbs} is higher than the transversal F^{sbs}. The difference between longitudinal and transversal specimens is over 10% for the means values. This implies that the material presents anisotropy in their SBS strength. The relatively lower strength in transversal direction may be associated to the fiber orientation and different residual stresses. The standard deviation in both directions resulted lower than 5%. All the quasi-static specimens presented interlaminar failure mode. However, the longitudinal specimens present complete separation of one aluminum face at one side of the loading nose

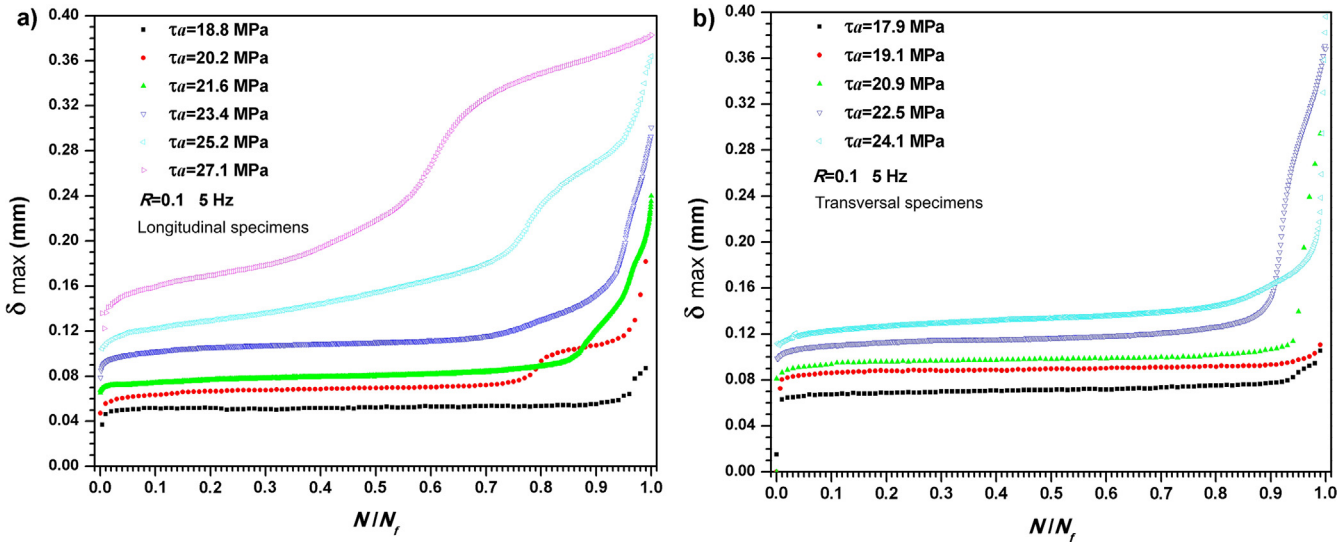

Fig. 5. Graph δmax-N/N_f of (a) longitudinal and (b) transversal specimens.

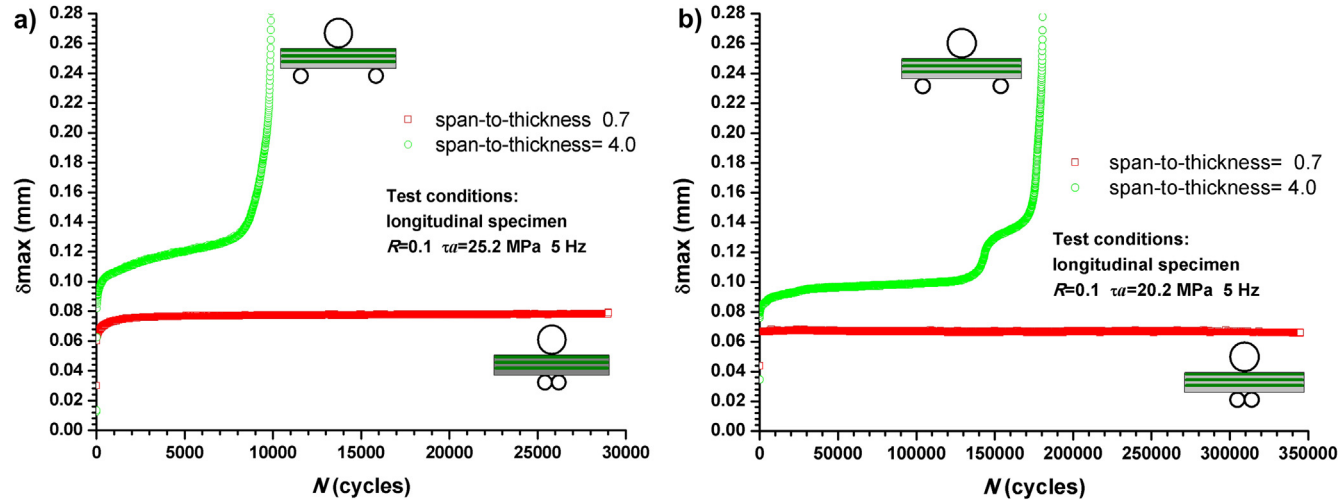

Fig. 6. Graphs δmax-*N* for longitudinal specimens with different span-to-thickness ratios at (a) τ_a = 25.2 MPa and (b) τ_a = 20.2 MPa.

(see Fig. 3c). The damage in these specimens was mainly in the interface Al-fiber/epoxy. The transversal specimens presented damage either through the glass/epoxy layer or in the interface Al-fiber/epoxy (see Fig. 3d).

Fig. 3a shows different SBS fatigue failure modes either by their orientation as for their stress level. In the case of the orientations, most failed longitudinal specimens presented failure mode type *e*, i.e., both interlaminar damage and a crack in the middle specimen span (see Fig. 3e). The inspection of the videos recorded along the tests showed that these specimens presented interlaminar damage that originated a progressive stiffness loss. In the last cycles a crack was nucleated in the middle span and grew through the specimen producing the collapse. This behavior can be explained as the damage and the change in the geometry modify the stress state in the specimen increasing the middle span stress and consequently a crack is nucleated in this zone leading to the final failure. This failure mode is considered valid because the specimens firstly presented interlaminar shear failure. Only one longitudinal specimen presented failure mode type *h*, as can be observed in Table 2.

Transversal specimens presented different failure modes at different τ_a values. Specimens that showed failure mode type *f* (only interlaminar shear) were observed at $\tau_a = 22.5$ MPa and 24.1 MPa (Fig. 3f). This failure mode is considered valid because the specimen failed by interlaminar shear. Failure mode type *g* was observed for fatigue life between 10^4 and $7 \cdot 10^5$ cycles (Fig. 3g) and type *h* between $5 \cdot 10^3$ and $2 \cdot 10^5$ cycles (Fig. 3h). Types *h* and *g* are considered valid because interlaminar shear damage was firstly observed and the cracks in the middle span and a support were observed at the end of the test. Type *i* was observed at low values of τ_a. This failure mode is considered invalid because the crack is nucleated near the support without previous interlaminar damage (Fig. 3i). As was commented in the result section, the crack grows through the Aluminum layer in the thickness direction of the specimen up to the fiber/epoxy layer. The specimen collapses by interlaminar shear when the crack reaches this layer. This failure mode prevents to obtain damage initiated by interlaminar shear at low load. A possible explanation of the occurrence of failure type *i* is that at high τ_a values the interlaminar shear damage nucleates and grows faster than the damage produced by supports. At low τ_a values the damage by supports nucleates and grows in first place. This type of failure was not observed in longitudinal specimens possibly by anisotropy in the fatigue behavior of the aluminum layer. This anisotropy may be associated to the post-curing rolling process that produces residual tensile stresses and strengthening in the longitudinal direction of the aluminum layer.

Anisotropy in the SBS fatigue life can be observed in Fig. 4 where only the assumed valid failure modes are presented. According to this figure, the SBS fatigue life is higher in the longitudinal direction. The scatter in the longitudinal direction is smaller than in the transversal one. The fitted curve of the form of Eq. (4) is used in this paper because it is one of the most common models used in tension-tension, tension-compression and compression-compression fatigue in composite materials [11,12], and it was previously employed in other SBS fatigue results [16,10]. The R^2 value is higher for longitudinal specimens than for transversal specimens. The exponential coefficients $1/k$ are quite similar for both curves. However, the curve of transversal specimens does not have results of specimens with SBS fatigue life over 10^6 cycles. Further, the curve of longitudinal specimens includes run-out values that are considered with the same weight that failed specimens. This can lead to a conservative fitted curve. Also for SBS fatigue, Makeev [16] reported $1/k$ values of 0.3493 and 0.3414 for E-glass fiber reinforced epoxy and IM7-carbon fiber reinforced epoxy respectively. The slopes of these curves are greater than the obtained in this study. In a previous study [10] $1/k$ values were obtained for E-glass reinforced polyester between 0.0575 and 0.0674. These last values are similar to the slopes obtained in this study.

The change in the maximum displacement, δmax, along the specimen fatigue life shows three stages, as can be observed in Fig. 5. Firstly, there is a transient where the rate of change of δmax decreases. Then, there is an approximately constant rate and finally δmax increases up to the failure. The size of each stage depends on the τ_a level. The third stage shows different patterns. The inspection of the videos shows different situations for this last stage. In some curves, δmax increases continuously because the crack in the specimen did too. In others curves a rapid increase of δmax followed by small increases is observed. This occurred in some specimens because the crack growth rate was initially fast followed of a reduced or null crack rate.

The change of δmax is used in this research as an indicator of damage accumulation in the specimen. This indicator does not allow to distinguish the failure mechanism. In the first stages of the fatigue life many failure mechanisms may be present, although only interlaminar shear damage was observed with the digital microscope. The complex stress state in the SBS specimen may produce other types of damage. The use of specimens with reduced span, i.e., supports closely together as possibly, is a common arrangement to obtain indentation correction in SE(B) fracture specimens [21]. They are used in this research to observe and measure the indentation along the fatigue test. Fig. 6 shows that indentation is important in a few first cycles. After the first cycles, the values of δmax remain practically unchanged. Even though the indentation may be negligible in the second stage, other mechanisms can be present. For example, the new local stress state product of the interlaminar shear damage progress through the fiber/epoxy or interface Al-fiber/epoxy may produce plastic deformation in the aluminum lamina.

SBS test is considered adequate in this research because this was simple, easy-to-use and it produces interlaminar shear damage in large part of the fatigue specimens and in all quasi-static specimens. In fatigue cases, the interlaminar damage was observed in the first stages of the fatigue life and the final failure was produced by other damage mechanisms. As previously mentioned, damage near a support instead of interlaminar shear was observed in the first life stage of transversal specimens at low τ_a values. Test device with larger diameters of supports may be a solution to this problem. However, premature compression jamming may be observed when the specimen loses stiffness. The results of SBS fatigue may be used as a technological characteristic of the material that provides information about the interlaminar shear fatigue and it can be used to compare materials.

A complete SBS fatigue characterization of the material will require tests at other *R*-values in order to build constant life-time diagrams (CLD) of SBS stresses. These tests at different *R*-values and other loading frequencies are under study as a continuation of this research.

5. Conclusions

SBS quasi-static and fatigue tests were performed in Glare 1 3/2 in two principal material orientations.

Quasi-static tests presented interlaminar shear failure mode and F^{sbs} in longitudinal orientation was higher than in transversal orientation.

Fatigue tests showed that the SBS fatigue strength in the longitudinal orientation was higher than in transversal orientation for the data evaluates. Longitudinal specimens presented interlaminar shear damage followed by crack growth in the middle span of the specimen. Transversal specimens presented diverse failure modes at different τ_a levels.

The use of reduced span in some fatigue specimens showed that the indentation effect was appreciable in the first fatigue cycles. Curves δmax-cycles are a good indicator of specimen damage but they do not give information about the damage mechanism.

SBS test was considered adequate in this research because it is simple and easy-to-use, and because it produced interlaminar shear damage in large part of the fatigue specimens and in all quasi-static specimens.

Acknowledgments

The authors wish to thanks CONICET for the permanent support. The authors also thank Enrique M. Castrodeza and Fernando L. Bastian (COPPE-UFRJ) for supplied the material and Eduardo G. Benotti (GMF-LPM) for his invaluable aid in the construction of the test devices.

Appendix A. Supplementary material

Supplementary data associated with this article can be found, in the online version, at http://dx.doi.org/10.1016/j.ijfatigue.2016.11.001.

References

[1] Schijve J. Development of fiber-metal laminates, ARALL and GLARE, new fatigue resistant materials; 1993.
[2] Vlot A, Gunnink JW, editors. Fibre metal laminates. Dordrecht, Netherlands: Springer; 2001. doi: http://dx.doi.org/10.1007/978-94-010-0995-9.
[3] Sinmazçelik T, Avcu E, Özgür M, Çoban O. A review: fibre metal laminates, background, bonding types and applied test methods. Mater Des 2011;32:3671–85. doi: http://dx.doi.org/10.1016/j.matdes.2011.03.011.
[4] Marissen R. Fatigue crack growth in ARALL: a hybrid aluminium-aramid composite material. Crack growth mechanisms and quantitative predictions of the crack growth rates. Delft University of Technology; 1988.
[5] Hosford WF. Mechanical behavior of materials. 2nd ed. Cambridge: Cambridge University Press; 2009.
[6] Alderliesten RC. Analytical prediction model for fatigue crack propagation and delamination growth in Glare. Int J Fatigue 2007;29:628–46. doi: http://dx.doi.org/10.1016/j.ijfatigue.2006.07.00.
[7] Structural Laminates Company. QA Reports No. B0319B-2, B1008B-1, B0904A-3. New Kensington, PA; 1994.
[8] ASTM International. ASTM D2344/D2344M-13, Standard Test Method for Short-Beam Strength of Polymer Matrix Composite Materials and Their Laminates; 2013. http://dx.doi.org/10.1520/D2344_D2344M.
[9] Pach E, Korin I, Ipiña JP. Simple fatigue testing machine for fiber-reinforced polymer composite. Int J Adv Manuf Technol 2012;36:76–82. doi: http://dx.doi.org/10.1111/j.1747-1567.2011.00713.x.
[10] Kotik H, Perez Ipiña J. Frequency effect in short-beam shear fatigue of a glass fiber reinforced polyester composite. Int J Fatigue 2016;90:116–24. doi: http://dx.doi.org/10.1016/j.ijfatigue.2016.04.025.
[11] ASTM International. ASTM E739-10(2015) Standard Practice for Statistical Analysis of Linear or Linearized Stress-Life (S-N) and Strain-Life (ε-) Fatigue Data. Annu B ASTM Stand 2015; i: 1–7. http://dx.doi.org/10.1520/E0739-10R15.
[12] Vassilopoulos AP. Fatigue life prediction of composites and composite structures. Boca Raton: CRC Press; 2010.
[13] Pipes R Byron. Interlaminar shear fatigue characteristics of fiber-reinforced composite materials. Compos Mater Test Des 1974;546:419–32.
[14] Bevan LG. Axial and short beam shear fatigue properties of cfrp laminates. Composites 1977;8:227–32.
[15] Roudet F, Desplanques Y, Degallaix S. Fatigue of glass/epoxy composite in three-point-bending with predominant shearing. Int J Fatigue 2002;24:327–37. doi: http://dx.doi.org/10.1016/S0142-1123(01)00088-3.
[16] Makeev A. Interlaminar shear fatigue behavior of glass/epoxy and carbon/epoxy composites. Compos Sci Technol 2013;80:93–100. doi: http://dx.doi.org/10.1016/j.compscitech.2013.03.013.
[17] ISO B. 14130-1998. Fiber-reinforced plastic composite apparent interlaminar shear strength by short beam method; 1998.
[18] Botelho EC, Silva RA, Pardini LC, Rezende MC. A review on the development and properties of continuous fiber/epoxy/aluminum hybrid composites for aircraft structures. Mater Res 2006;9:247–56. doi: http://dx.doi.org/10.1590/S1516-14392006000300002.
[19] Park SY, Choi WJ, Choi HS. A comparative study on the properties of GLARE laminates cured by autoclave and autoclave consolidation followed by oven postcuring. Int J Adv Manuf Technol 2010:605–13. doi: http://dx.doi.org/10.1007/s00170-009-2408-x.
[20] Adams DF, Lewis EQ. Experimental study of three- and four-point shear test specimens. J Compos Technol Res 1995;17:341–9.
[21] ASTM International. ASTM D6068-10: standard test method for determining J-R curves of plastic materials; 2010. http://dx.doi.org/10.1520/d6068-10.